Spectrochimica Acta Part A: Molecular and Biomolecular Spectroscopy 353 (2026) 127572

Contents lists available at ScienceDirect

Spectrochimica Acta Part A: Molecular and Biomolecular Spectroscopy

journal homepage: www.journals.elsevier.com/spectrochimica-acta-part-a-molecular-and-biomolecular-spectroscopy

# Data science meets FTIR Imaging: a promising probe to improve the diagnosis of human uterine muscle lesions

Chiara Santoni [a,1], Giulia Orilisi [b,1], Stefania Greco [c], Valentina Notarstefano [d], Giovanni Delli Carpini [e], Abel Duménigo Gonzàlez [c], Federica Giantomassi [f], Alessandra Filosa [f], Gaia Goteri [f], Andrea Ciavattini [e], Gian Franco Zannoni [g], Giovanna Orsini [b], Elisabetta Giorgini [a,*], Pasquapina Ciarmela [c]

[a] Department of Life and Environmental Sciences, Polytechnic University of Marche, 60131 Ancona, Italy
[b] Department of Odontostomatologic and Specialized Clinical Sciences, Polytechnic University of Marche, 60126 Ancona, Italy
[c] Department of Experimental and Clinical Medicine, Polytechnic University of Marche, 60126 Ancona, Italy
[d] Department of Bioscience and Agro-Food and Environmental Technology, University of Teramo, 64100 Teramo, Italy
[e] Department of Clinical Sciences, Polytechnic University of Marche, 60126 Ancona, Italy
[f] Department of Biomedical Sciences and Public Health, Polytechnic University of Marche, 60126 Ancona, Italy
[g] Division of Anatomic Pathology and Histology, Università Cattolica del Sacro Cuore, "Agostino Gemelli" School of Medicine, 00168 Rome, Italy

## HIGHLIGHTS

- The study aims to improve the differential diagnosis of uterine tumors.
- Leiomyosarcoma (LMS) and leiomyoma histotypes (LMs) were analyzed by FTIRI.
- FTIRI is a high-resolution imaging technique for the analysis of tumor lesions.
- IR data were validated with statistical tools.
- Reliable spectral features for distinguishing LMS and LMs subtypes were achieved.

## GRAPHICAL ABSTRACT

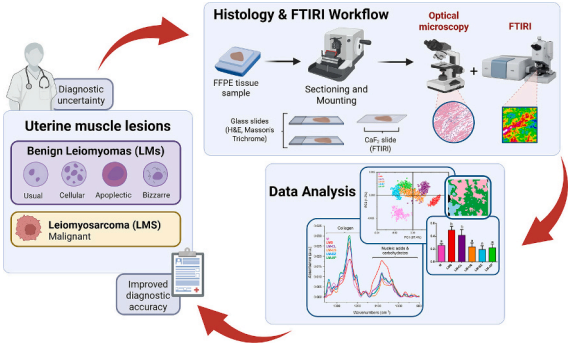


## ARTICLE INFO

*Keywords:*
Uterine leiomyomas
Leiomyosarcoma
Collagen
Fourier Transform InfraRed Imaging spectroscopy
Histology
Multivariate analysis

## ABSTRACT

Uterine smooth muscle tumors include a broad range of neoplasms, from benign leiomyomas (LMs) to malignant leiomyosarcomas (LMS), as well as intermediate forms classified as Smooth Muscle Tumors of Uncertain Malignant Potential (STUMP). An accurate diagnosis of these tumor types is essential for their appropriate clinical management; however, it remains challenging due to possible overlapping of histological features. In this study, a multidisciplinary approach combining Fourier Transform Infrared Imaging (FTIRI) spectroscopy, a label-free and non-destructive analytical technique, with histology and statistical analyses have been exploited for investigating the morpho-chemical characteristics of these uterine smooth muscle tumors. The analysis aimed to identify new reliable and diagnostic spectral markers, complementary to traditional histology, and thus useful for

* Corresponding author.
*E-mail address:* e.giorgini@staff.univpm.it (E. Giorgini).
[1] These Authors equally contributed to the study.

https://doi.org/10.1016/j.saa.2026.127572
Received 5 September 2025; Received in revised form 9 December 2025; Accepted 7 February 2026
Available online 11 February 2026

improving accuracy in cases with uncertain morphological features. Tissue samples including different leiomyoma histological subtypes, such as usual, cellular, apoplectic, and bizarre, were analyzed and compared with LMS and healthy myometrium. The analysis of IR data, submitted to univariate and multivariate statistical approaches, such as Principal Component Analysis (PCA) and Hierarchical Cluster Analysis (HCA), revealed distinctive spectral profiles associated with each tumor type and indicated changes in collagen content and organization as key features for a reliable discrimination not only between benign and malignant tissues but also among different LM histotypes.

## 1. Introduction

Leiomyomas and leiomyosarcomas are uterine smooth-muscle tumors characterized by very different biological behaviors, going from benign to malignant outcomes [1]. Leiomyomas are benign lesions which present several histological variants. The most common form is the usual-type, which accounts for the majority of cases; it is often asymptomatic or associated with symptoms such as abnormal uterine bleeding, pelvic pain, or infertility [2,3]. Other variants include the cellular and apoplectic types and, to a further extent, the less common but diagnostically challenging bizarre nuclei one [4]. On the malignant end, leiomyosarcoma is a rare and aggressive tumor characterized by high recurrence rates and poor prognosis [5,6].

From the histological point of view, usual-type leiomyomas are typically well-circumscribed lesions composed of monomorphic spindle-shaped cells arranged in intertwined fascicles. These fascicles are often separated by variable amounts of hyalinized collagen, which may subdivide the tumor into nodular structures. Cells show abundant eosinophilic cytoplasm and uniform, cigar-shaped nuclei with small nucleoli and rare mitotic figures. [1]. Cellular-type leiomyomas are characterized by increased cellularity, with round to oval cells displaying scant cytoplasm, and often lack the characteristic fascicular architecture seen in the usual-type. Prominent vascularization and the presence of stromal clefts are typical histological features [1]. In the bizarre variant, cells with markedly atypical, hyperchromatic nuclei, often multiple, and abundant eosinophilic cytoplasm are present. These tumors may exhibit degenerative vascular changes and chronic inflammatory infiltrates, although they generally lack significant mitotic activity or necrosis [7]. The apoplectic variant shows stellate hemorrhagic areas and edema within hypercellular smooth muscle nodules; abnormal blood vessels are commonly observed [1,8]. The malignant leiomyosarcoma is characterized by the occurrence of three major features: coagulative tumor cell necrosis, significant cytologic atypia, and a high mitotic index. The simultaneous presence of all three is required for a definitive diagnosis [9,10].

Up to date, the diagnosis of these lesions mainly relies on the most common non-invasive imaging techniques, such as ultrasound, magnetic resonance imaging, computed tomography, and positron emission tomography. The first diagnostic approach is usually based on ultrasound examination: it has the advantage of being easily accessible but provides little information on the degree of malignancy of the lesion [11]. The next step is magnetic resonance imaging, the most informative technique for a more in-depth characterization of uterine tissues. In fact, it allows for better discrimination against the nature of the lesion by highlighting the presence of irregular or infiltrative margins [12,13]. Recently, successful results have been obtained in the detection of metastasis by exploiting a combined approach based on PET and CT [14].

These pathologies pose a challenge because sometimes they can present quite similar clinical, radiological, and, to a further extent, histopathological features. This makes it difficult to reach a precise diagnosis, especially in the early stages, enabling one to distinguish benign from malignant lesions. To address this diagnostic gray zone, the World Health Organization (WHO) 2014 classification introduced and refined the category of Smooth Muscle Tumors of Uncertain Malignant Potential (STUMP) [15]. This category includes tumors that do not meet the full criteria for malignancy but also cannot be confidently diagnosed as benign [16,17]. Notably, bizarre nuclei leiomyomas are frequently included in this category due to their marked cytologic atypia, which resembles that observed in LMS, despite lacking other malignant features [15,18].

This diagnostic uncertainty underscores the urgent need for more objective and reliable markers to improve the classification and management of uterine smooth muscle tumors. In recent years, molecular studies have aimed to identify biomarkers capable of distinguishing benign from malignant lesions and clarifying the status of STUMP [19]. In this context, two molecules, Raf Kinase Inhibitor Protein (RKIP) and hypusinated eIF5A, have been proposed as potential diagnostic markers to differentiate between benign and malignant uterine smooth muscle tumors [20,21].

In the last decades, Fourier Transform Infrared Imaging (FTIRI) spectroscopy has emerged as a powerful, label-free analytical tool. Indeed, FTIRI has been applied to study tumor samples in several human districts, including the oral cavity [22,23], prostate [24], lung [25], gut [26], breast [27], skin [28], etc. By coupling the potential of optical microscopy with advanced array detectors, this technique allows to map micrometric areas, collecting at the same time and on the same sample the microphotograph and the IR image, in which each pixel corresponds to an IR spectrum. Hence, it is possible to obtain a morpho-chemical characterization of the sample, by associating the topographical distribution and composition of the main macromolecules (such as proteins, lipids, nucleic acids, carbohydrates, etc.) to the tissue structure [29]. Recently, some Authors of our have successfully applied FTIRI to elucidate the biochemical characterization of uterine fibrotic diseases, providing valuable insights into the structural organization of the extracellular matrix (ECM) and its components, particularly collagen [30].

Based on these interesting results, in the present study we propose a multidisciplinary approach coupling FTIRI spectroscopy, histological analysis and statistical methods (both multivariate and univariate), to distinguish uterine smooth muscle lesions, with particular attention to the differentiation not only between leiomyosarcoma and leiomyomas, but also among the different leiomyomas. The final goal is to contribute to the development of additional objective, image-based diagnostic criteria that may complement histopathological evaluation and improve diagnostic accuracy in challenging cases.

## 2. Materials and methods

### 2.1. Samples' collection

Tissue samples were derived from Pathological Anatomy Laboratory, Azienda Ospedaliera Ospedali Riuniti di Ancona, Università Politecnica delle Marche, Ancona and from Department of Woman and Child Health, Fondazione Policlinico Universitario A. Gemelli IRCCS, Rome. Permission was granted by the Human Investigation Committee of Marche (protocol code MORFO-GF, validated on November 14th, 2024).

The following samples were investigated: N. 5 samples of leiomyosarcoma (LMS group); N. 5 samples of leiomyoma with cellular histotype (LM-CL group); N. 5 samples of leiomyoma with usual histotype (LM-US group); N. 3 sample of leiomyoma with apoplectic histotype (LM-AP group), and N. 3 samples of leiomyoma with bizarre histotype (LM-BZ

group). N. 3 samples of healthy myometrium (M) were also included as control group.

From each sample, three serial sections (~ 5 μm thickness) were cut, two were deposited onto glass slides for the histological analysis and the third onto $CaF_2$ optical window (38 mm × 26 mm × 1 mm size) for the FTIR Imaging analysis. The use of different sections for histological and FTIRI analyses relies on the fact that FTIR spectroscopy is an absorption technique and requires specific optical supports transparent to IR radiation. Moreover, the histological images acquired in whole sections guided the selection of the areas for the acquisition of IR images.

### 2.2. Histological analysis

A Masson's trichrome staining kit with aniline blue (Bio-Optica, Milan, Italy) was used, following the procedure reported in literature [30]. This staining let investigate the consistency and amount of the extracellular matrix and in particular of collagen, which resulted light blue colored. Stained sections were analyzed by an Olympus BM50 optical microscope (Olympus, Japan), with 20× magnification to capture the overviews of all sections.

### 2.3. Acquisition of IR images and data analysis

An INVENIO-R interferometer, coupled with a Hyperion 3000 Vis-IR microscope and equipped with a Focal Plane Array (FPA) detector operating at liquid nitrogen temperature (Bruker Optics, Ettlingen, Germany) was used. The FPA detector lets acquire IR images of non-homogeneous biological samples, such as tissues and cells, providing a contemporary morpho-chemical analysis. On each section, air dried for 20 min, 2 or 3 IR images were acquired, based on information from the histological images: the number of IR images collected on each section depended on how many areas worthy of investigation were detected.

IR data were collected in transmission mode in the 4000–900 $cm^{-1}$ range, with a spectral resolution of 4 $cm^{-1}$; each IR image was 164 × 164 $\mu m^2$ size and it was composed by 4096 pixel/spectra, with a spatial resolution of 2.56 × 2.56 $\mu m^2$/pixel; each spectrum was the result of 256 scans. Before collecting the IR image of each sample, the background spectrum was acquired on a clean area of the $CaF_2$ optical window. Raw IR images were then subjected to the Atmospheric Compensation and Vector Normalization routines in the whole spectral range of acquisition, respectively for discarding the contribution of atmospheric carbon dioxide and water vapor and avoiding artifacts deriving from thickness differences. The acquisition of IR images and all the spectral treatments were performed by the software OPUS 7.1 (Bruker Optics, Ettlingen, Germany).

Pre-processed IR images thus obtained were first integrated under the 1360–1185 $cm^{-1}$ spectral region, to obtain false color maps representing the topographical distribution and relative amount of collagen. To build false color maps, an arbitrary color scale was used, with white/pink colors indicating areas with the highest absorbance *v*alues, and blue those with the lowest ones.

Pre-processed IR images were then submitted to Hierarchical Cluster Analysis (HCA), by using the Euclidean distance and the Ward's method (CytoSpec software v. 2.00.01). This procedure lets identify, within the mapped areas, points characterized by the same spectral profile, named spectral clusters.

Based on false color images and HCA clusters, for each experimental group, ca. 250 IR spectra were extracted on areas with the major amount of collagen. These spectral data sets were first submitted to an exploratory analysis by means of Principal Component Analysis (PCA), that linearly transforms the spectral data onto a new coordinate system, in which the position of each spectrum (showed as a function of the principal components) easily highlights the largest variation within the data set (OriginPro 2023 software). PCA was performed on absorbance spectra in the 1360–1185 $cm^{-1}$ and 1185–900 $cm^{-1}$ ranges, upon vector normalization and two-points baseline correction (Vector Normalization and Baseline Correction routines, OPUS 7.1 software, Bruker Optics, Ettlingen, Germany).

Then, the average IR spectrum and the corresponding standard deviation spectra of each spectral population were calculated, submitted to vector normalization (Averaging and Vector Normalization routines, OPUS 7.1 software, Bruker Optics, Ettlingen, Germany), and curve fitted in the 1360–900 $cm^{-1}$ region (Peak Fitting routine; GRAMS/AI 9.1, Galactic Industries, Inc., Salem, New Hampshire). This procedure allows to identify all the peaks underlying a convoluted band, in terms of position (wavenumber, $cm^{-1}$), height and area. The fitting was performed upon local straight baseline correction in the above defined ROI (regions of interest). The number and position of the underlying peaks were identified by the analysis of second derivative minima and fixed during the fitting procedure by means of Gaussian functions (GRAMS/AI 9.1, Galactic Industries, Inc., Salem, New Hampshire) (see Fig. 1S in Supplementary Material). The integrated areas of meaningful peaks were used to calculate specific spectral parameters.

### 2.4. Statistical analysis

Statistical analysis was performed by PRISM 8.0 software (GraphPad Software, San Diego, CA). IR data were presented as mean ± standard deviation. Significant statistical differences among groups were calculated by means of One-way ANOVA multiple comparison test; statistical significance was set at $p < 0.05$.

## 3. Results

### 3.1. High resolution imaging analysis

Masson's trichrome staining was used to identify various tissue components thanks to their different coloration, such as collagen (blue/cyan), muscle fibers (pink), and cytoplasm and cell nuclei (red/brown). Based on this evidence, the analysis of the histological images of representative samples of leiomyosarcoma (LMS) (Fig. 1A), leiomyomas with cellular (LM-CL), usual (LM-US), apoplectic (LM-AP) and bizarre (LM-BZ) histotypes (respectively Fig. 1B–E), and healthy myometrium (M) (Fig. 1F) revealed interesting differences among groups. More in detail, collagen was almost absent in LMS being mainly localized in isolated spots, surrounding blood vessels (Fig. 1A). Regarding LM samples, a few amount of collagen was found in LM-CL (Fig. 1B), while higher quantities were observed in LM-US, LM-BZ and LM-AP. Interestingly, a different distribution was also evidenced: in LM-US collagen was characterized by a poor structural organization (Fig. 1C); in LM-BZ, it appeared not homogeneously distributed (Fig. 1D), whereas, in LM-AP, it resulted in a more uniform arrangement (Fig. 1E).

The hyperspectral analysis performed on serial unstained sections is displayed in Fig. 2. Specifically, the microphotographs of representative sections of each experimental group are shown in Fig. 2A (red boxes indicating the areas selected for IR mapping), while in Fig. 2B, the corresponding false color images describing the topographical distribution of collagen are reported. Interestingly, this analysis corroborated the above-described histological results. In LMS, a minimal amount of collagen was observed, distributed in a punctate manner, likely due to the tumor's infiltration into the surrounding tissue, while an increasing amount of this protein was found going from LM-CL to LM-US, LM-BZ, and LM-AP. The presence of different spectral populations emerged by HCA images (Fig. 2C), in which pink clusters co-localized with collagen-rich areas highlighted by false color images, while green ones were more consistent with the presence of cells.

For deepening the different spectral features among groups, the spectral region 1360–900 $cm^{-1}$, representative of collagen, phosphates and nucleic acids was further investigated (Fig. 3). The most meaningful peaks are listed in Table 1. Interestingly, in M and LM samples, the following bands representative of collagen were found: ~1340 $cm^{-1}$ (wagging of $CH_2$ groups in proline, the main amino acid in collagen)

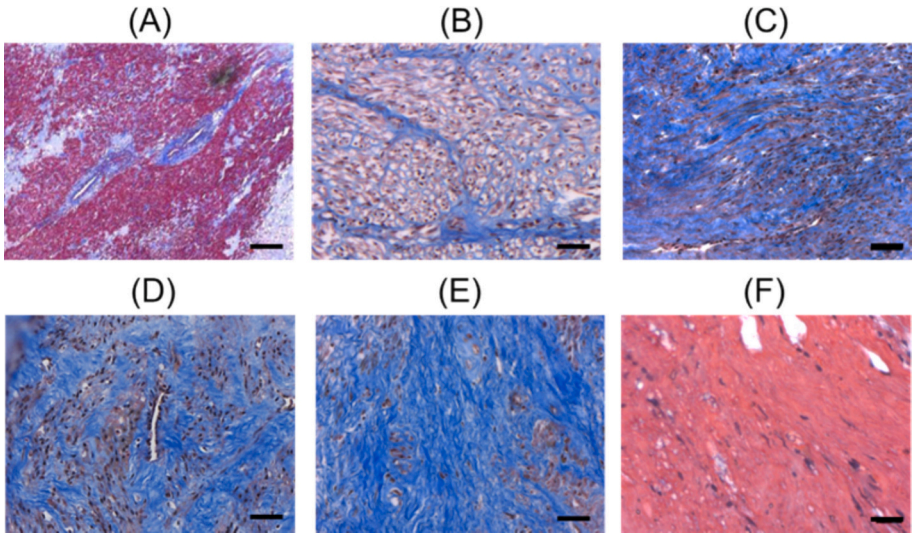


**Fig. 1.** Masson's trichrome histological images of the following uterine human lesions: (A) leiomyosarcoma (LMS); leiomyomas with (B) cellular (LM-CL), (C) usual (LM-US), (D) bizarre (LM-BZ), and (E) apoplectic (LM-AP) histotypes; (F) healthy myometrium (M) (scale bar 50 μm). Collagen (blue/cyan), muscle fibers (pink), and cytoplasm and cell nuclei (red/brown). (For interpretation of the references to color in this figure legend, the reader is referred to the web version of this article.)

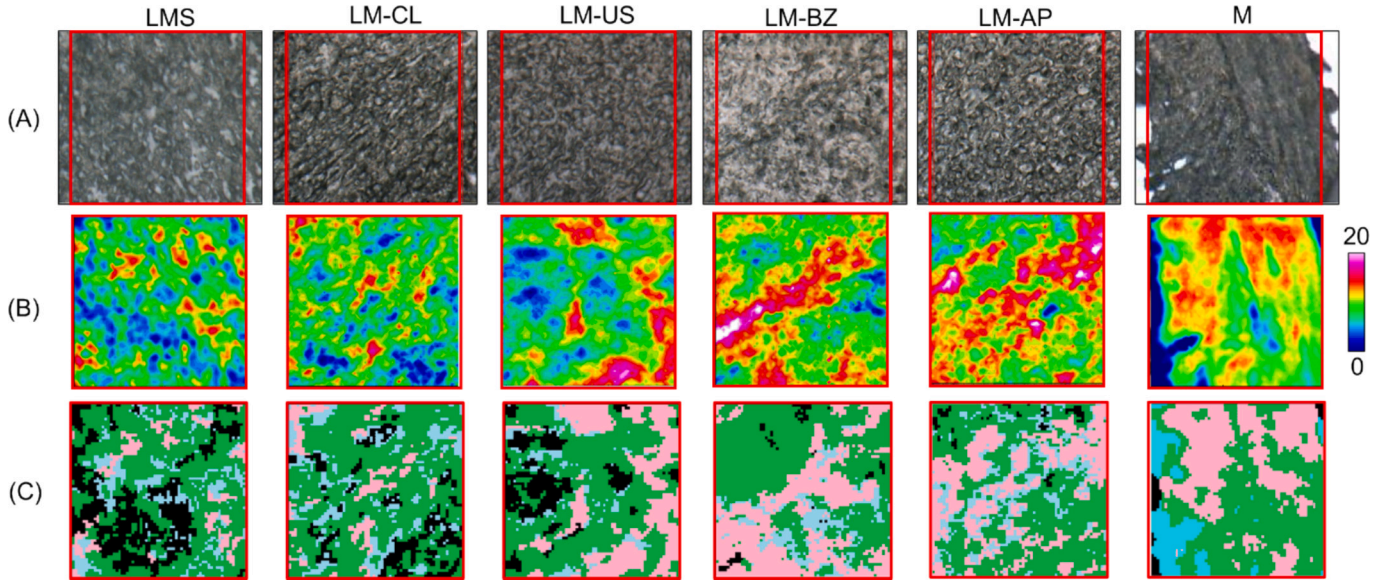


**Fig. 2.** Hyperspectral analysis of representative sections of healthy myometrium (M), leiomyosarcoma (LMS), and leiomyoma samples with cellular (LM-CL), usual (LM-US), bizarre (LM-BZ), and apoplectic (LM-AP) histotypes. (A) Microphotographs showing the IR mapped areas (highlighted by red boxes; 164 × 164 $mm^2$ size; 4096 pixel/spectra with spatial resolution 2.56 × 2.56 $\mu m^2$/pixel). (B) False color images describing the spatial distribution of collagen (an arbitrary color scale ranging from 0 to 20 in terms of absorbance was used, with white/pink colors indicating areas with the highest absorbance values in the 1360–1185 $cm^{-1}$ region, while blue those with the lowest ones). (C) HCA images showing the localization of different spectral populations (pink clusters, collagen rich areas; green clusters, cellulated regions; cyan, not defined; black, areas without sample). (For interpretation of the references to color in this figure legend, the reader is referred to the web version of this article.)

[22,31]; ~1320 $cm^{-1}$ (α-helix secondary structures) [22]; ~1284 $cm^{-1}$, and ~ 1240 $cm^{-1}$ (triple helix secondary structures) [32,33]; ~1260 $cm^{-1}$ (random coil structures) [32,33]; ~1203 $cm^{-1}$ (amino acids' lateral chains) [34]; ~1157 $cm^{-1}$ (COH moiety) [35,36], and ~ 1030 $cm^{-1}$ (glycogen and carbohydrates) [37]. A different shape was displayed by LMS, in which the absence of the bands at ~1284 $cm^{-1}$ and ~ 1203 $cm^{-1}$ confirmed the lack of collagen. This malignant lesion was characterized by a prominent band at ~1080 $cm^{-1}$, attributable, together with those at ~1240 $cm^{-1}$ and ~ 1220 $cm^{-1}$, to the stretching modes of phosphates in nucleic acids [38,39], a shoulder at ~1122 $cm^{-1}$ [38,39], due to C—O of ribose in RNA, and a peak at ~968 $cm^{-1}$, corresponding to the backbone vibration of DNA [38,39]. Interestingly, a weak but well evident peak at ~1170 $cm^{-1}$ was also present, due the stretching vibration of non-hydrogen bond C—O, mainly in protein component [35,36,40,41].

### 3.2. Collagen features

The analysis of the PC scores plot, performed on absorbance spectra in the 1360–1185 $cm^{-1}$, diagnostic for collagen, confirmed a different macromolecular composition in the extracellular matrix of the analyzed groups (Fig. 4A). A good separation was found among all spectral populations, letting distinguish healthy myometrium (M) from benign (LMs) and malignant (LMS) lesions. Specifically, M and LMS were localized

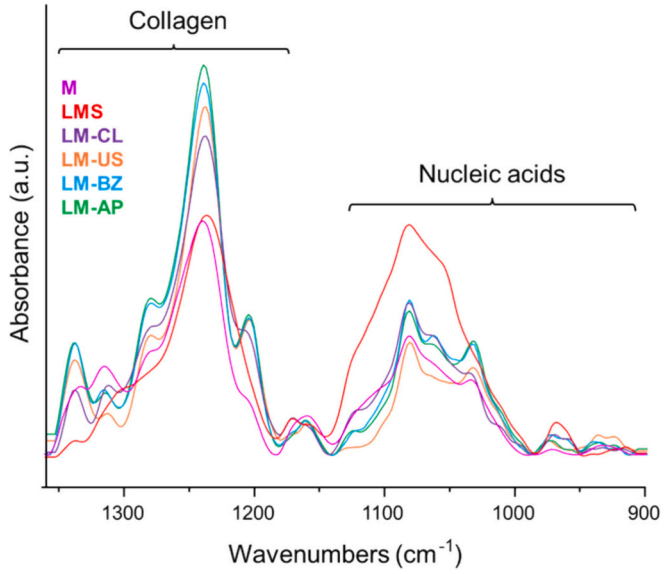


**Fig. 3.** Representative spectral profiles of myometrium (M), leiomyosarcoma (LMS) and leiomyoma with bizarre (LM-BZ), apoplectic (LM-AP), usual (LM-US), and cellular (LM-CL) histotypes. Spectra are displayed in absorbance mode in the 1360–900 $cm^{-1}$ region.

**Table 1**
Major IR peaks detected in healthy myometrium (M), leiomyosarcoma (LMS) and leiomyomas (LM-CL, LM-US, LM-BZ and LM-AP): position (wavenumbers, $cm^{-1}$), vibrational mode, and biological meaning.

| Wavenumbers ($cm^{-1}$) | Vibrational modes | Biological meaning |
|---|---|---|
| ~1340 | Wagging of $CH_2$ moieties | Proline |
| ~1320 | Alpha helix structures | Collagen |
| ~1284, ~1240 | Triple helix structures | |
| ~1260 | Random coil structures | |
| ~1203 | Amino acids' side chains | |
| ~1170, ~1157 | Respectively non H-bond and H-bond $\nu$C-O | non H-bond and H-bond C—O groups, mainly in proteins |
| ~1122 | $\nu$C-O of ribose | RNA |
| ~1240, ~1220, ~1080 | $\nu_{asym}$ and $\nu_{sym}$ $PO_2^-$ | Nucleic acids |
| ~1030 | δC-O-H, $\nu$C-O, and $\nu$C-C | Glycogen |
| ~997 | $\nu$ uracil ring | RNA |
| ~968 | DNA backbone vibration | DNA |
| ~935 | Z-DNA vibration | Z-DNA |

respectively in the third and fourth quadrants, segregated each other along PC1 (explained variance 97.4%), with the most discriminant spectral features at ~1340 $cm^{-1}$, ~1284 $cm^{-1}$ and ~ 1240 $cm^{-1}$ (PC1 loadings; Fig. 4B). LM histotypes were found in the upper part of the plot, segregated from M and LMS along PC2 (explained variance along 1.3%). Moreover, LM-CL was on the first quadrant, LM-AP and LM-BZ on the second one, while LM-US shows an intermediate position. The PC2 loadings displayed as the most discriminant spectral features the peaks centered at ~1320 $cm^{-1}$, and ~ 1220 $cm^{-1}$ (Fig. 4B).

To identify reliable spectral markers able to distinguish between different leiomyomas, specific collagen features were investigated in M and LM samples (LMS was not included due to the very scarce presence of collagen) (Fig. 5). The spectral parameter PROLINE (integrated area of the band at ~1340 $cm^{-1}$) is representative of the relative amount of proline, the most abundant amino acid in collagen, and, hence, of collagen [22,31]: it confirmed what already pinpointed by histological and hyperspectral analyses, with the highest values in LM-BZ and LM-AP, followed by LM-US, M, and LM-CL (Fig. 5A). With regard to collagen secondary structure, the following spectral parameters were investigated: ALPHA HELIX (integrated area of the band at ~1320 $cm^{-1}$) [22]; TRIPLE HELIX (integrated area of the band at ~1284 $cm^{-1}$) [32,33]; RANDOM (integrated area of the band at ~1260 $cm^{-1}$) [32,33], and FOLDED/UNFOLDED (ratio between the integrated area of the band at ~1284 $cm^{-1}$, representative of triple helix structures, and ~ 1260 $cm^{-1}$, representative of random coil structures). ALPHA HELIX agreed with PROLINE: the lowest value was displayed by LM-CL, while the highest ones were found in LM-BZ and LM-AP (Fig. 5B). TRILPE HELIX (Fig. 5C) and RANDOM (Fig. 5D) showed an inverted trend, suggesting a higher structural organization of collagen in M, LM-CL and LM-US respect to LM-BZ and LM-AP, as confirmed also by FOLDED/UNFOLDED (Fig. 5E).

### 3.3. Analysis of the cellular component

The analysis of the PC scores plot (Fig. 6A), performed in the 1185–900 $cm^{-1}$ range, showed the distribution of different uterine tissue types along the first two principal components (PC1: 75.2%, PC2: 8.0%). The plot highlighted a clear separation between healthy myometrium (M, pink) and leiomyosarcomas (LMS, red), predominantly segregated along PC1. M spectra were mainly located on the left side of the plot (negative PC1), while LMS ones occupied the right-lower quadrant, indicating distinct spectral features between these two tissue types. The corresponding PC1 loadings (Fig. 6B) showed that this separation was mainly driven by spectral bands at ~1125 $cm^{-1}$, ~1080 $cm^{-1}$, and ~ 1030 $cm^{-1}$, suggesting biochemical alterations in the extracellular matrix or cellular content of LMS compared to M. Benign leiomyomas (LMs) exhibited greater variability: LM-AP (green), LM-BZ (cyan), were mostly clustered in the upper part of the plot (positive PC2), while LM-US (orange) and LM-CL (purple) were interspersed among LMS samples, showing less defined clusters and suggesting intermediate or overlapping biochemical characteristics. PC2 loadings indicated that this separation was mainly influenced by peaks at ~1170 $cm^{-1}$, ~1080 $cm^{-1}$ and ~ 968 $cm^{-1}$.

To identify spectral markers able to improve the diagnosis of LMS respect to LM histotypes, specific spectral parameters related to the cellular component were also analyzed: PHOSPHATES (integrated area of the band at ~1080 $cm^{-1}$) [38,39]; DNA (integrated area of the band at ~968 $cm^{-1}$) [38,39]; RNA (integrated area of the band at ~1122 $cm^{-1}$) [38,39]; GLYCOGEN (integrated area of the band at ~1030 $cm^{-1}$) [37]; NON H-BOND/H-BOND C—O (ratio between the integrated areas of the bands at ~1170 $cm^{-1}$ and ~ 1157 $cm^{-1}$) [35,36,40,41]. The statistical analysis of the above defined spectral parameters let draw some considerations: (i) LMS and LM-CL were characterized by the highest values of PHOSPHATES, DNA and RNA, suggesting the presence of a highly cellulated and actively proliferating tissue (Fig. 7A–C); lower values in these parameters were found in the other LMs, with a decrement going from LM- US, LM-BZ, LM-AP and M, indicating a progressive decrease in cell content; (ii) GLYCOGEN was lowest in LMS (Fig. 4.7D), while it increased in a statistically significant manner when moving from M and LM-CL to LM-US, LM-BZ and LM-AP; this result suggests a higher consumption of sugars in LMS due to the presence of actively proliferating cells; (iii) LMS displayed also the highest value of NON H-BOND/H-BOND C—O (Fig. 7E), suggesting an increase of the band at ~1170 $cm^{-1}$, already observed in tumor samples.

## 4. Discussion

Uterine smooth muscle tumors encompass a spectrum of neoplasms with markedly different biological behavior, ranging from benign leiomyomas (LM) to malignant leiomyosarcomas (LMS), with intermediate entities such as STUMPs [1,15]. Among benign leiomyomas, several histological variants exist, including usual (LM-US), cellular (LM-CL), bizarre (LM-BZ), and apoplectic (LM-AP), which occasionally display features overlapping with malignant lesions, thus complicating the diagnostic process [4].

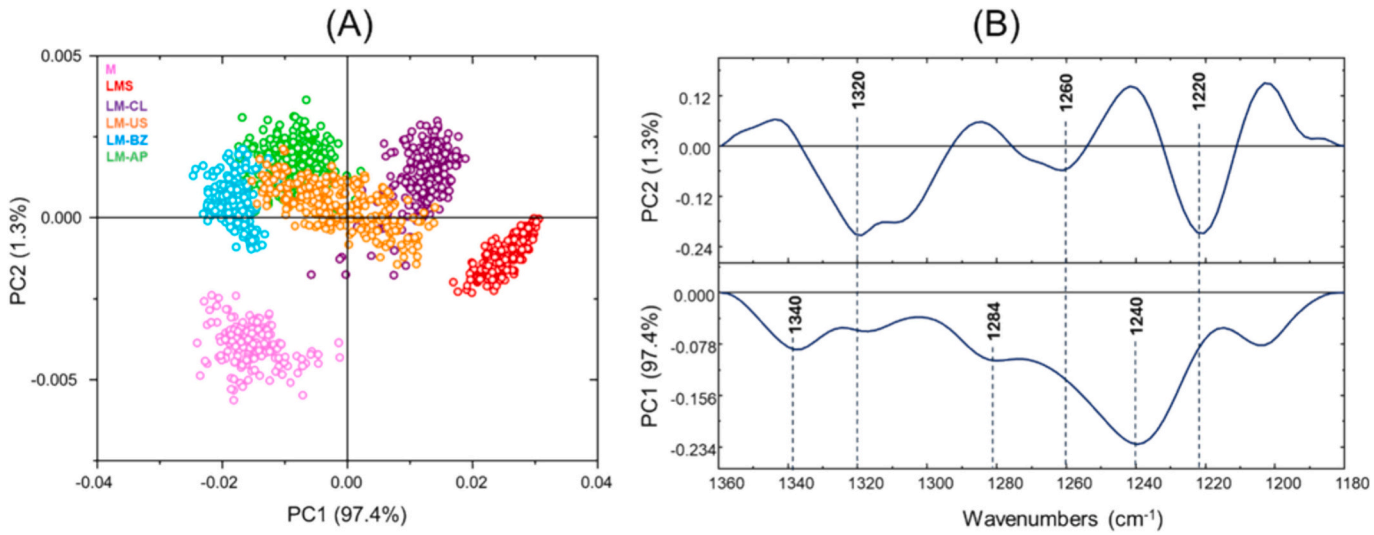


**Fig. 4.** (A) PCA scores plot calculated in the 1360–1185 $cm^{-1}$ on absorbance spectral populations of healthy myometrium (M), leiomyosarcoma (LMS), and leiomyoma samples with cellular (LM-CL), usual (LM-US), bizarre (LM-BZ), and apoplectic (LM-AP) histotypes. (B) PC1 and PC2 loadings.

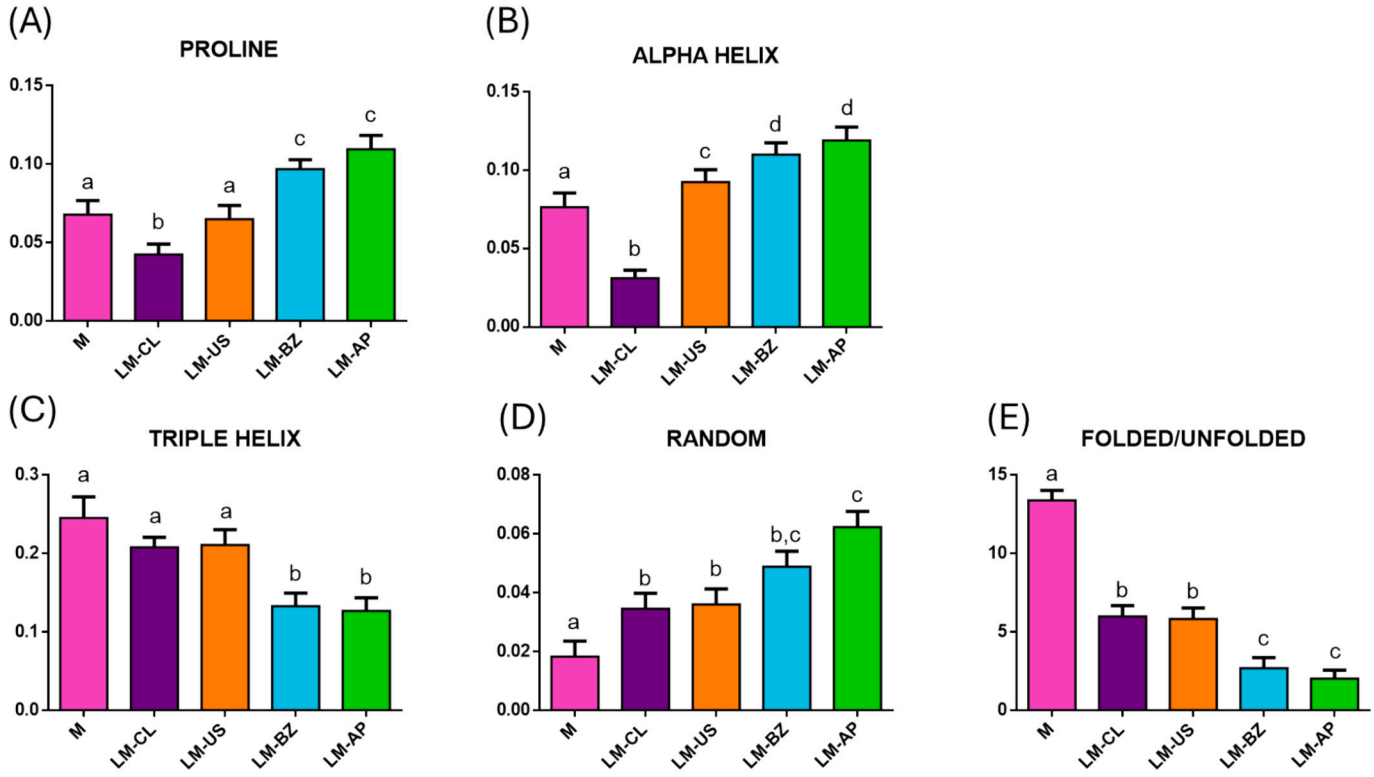


**Fig. 5.** Statistical analysis of the following spectral parameters: (A) PROLINE (representative of the relative amount of proline); (B) APLHA HELIX (representative of alpha helix structures); (C) TRIPLE HELIX (representative of triple helix structures); (D) RANDOM (representative of random coil structures), and (E) FOLDED/UNFOLDED (ratio between folded and unfolded structures). Data are presented as mean ± SD. Different lowercase letters over histograms indicate statistically significant difference among M, LM-CL, LM-US, LM-BZ, and LM-AP (One-way ANOVA; Tukey's multiple comparisons test; statistical significance was always set at $p < 0.05$; GraphPad software, San Diego, CA).

In recent years, FTIRI spectroscopy has emerged as a promising tool in the biomedical field, thanks to its ability to probe the biochemical composition and structural organization of tissues [22–30]: it has been demonstrated that by detecting vibrational signatures of the main biological macromolecules, FTIR can provide label-free, non-destructive insights into molecular alterations associated with pathological changes, including Usual type leiomyoma [22,30].

Building upon this potential, in the present study, leiomyosarcoma and different variants of leiomyoma have been investigated combining FTIRI spectroscopy, histology, and statistical analyses. This multidisciplinary approach allowed us to further explore the structural information from histology with that at the molecular level via FTIRI, providing a thorough understanding of the nature of the different lesions. The focus was on characterizing the extracellular matrix, particularly collagen, and the cellular component, to identify spectral markers capable of supporting differential diagnosis, mainly in challenging cases.

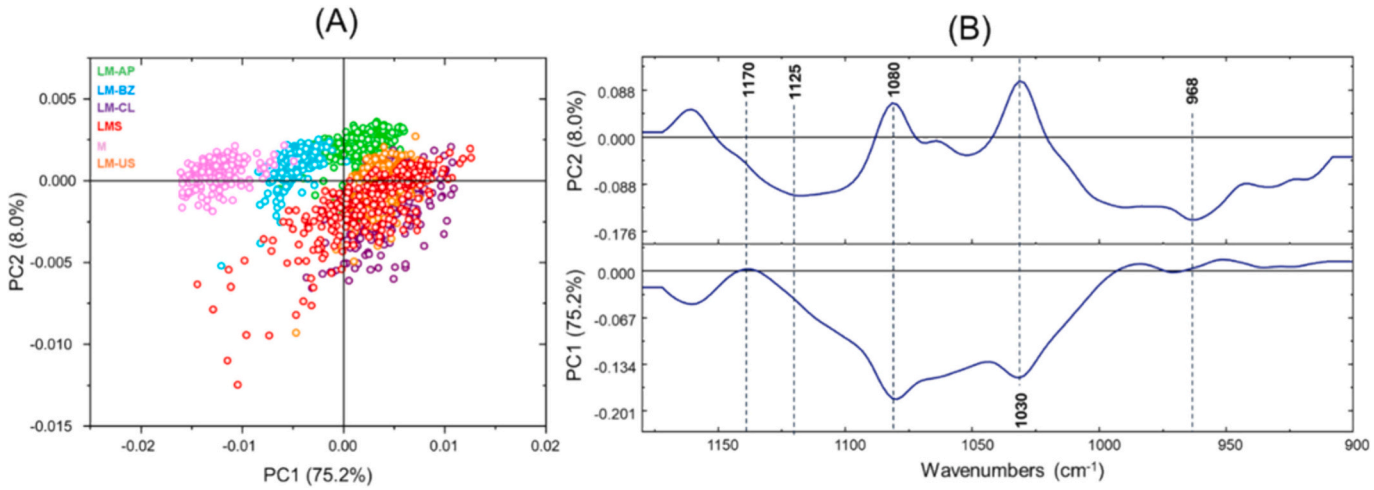


**Fig. 6.** (A) PCA scores plot calculated in the 1185–900 $cm^{-1}$ on absorbance spectral populations of healthy myometrium (M), leiomyosarcoma (LMS), and leiomyoma samples with cellular (LM-CL), usual (LM-US), bizarre (LM-BZ), and apoplectic (LM-AP) histotypes. (B) PC1 and PC2 loadings.

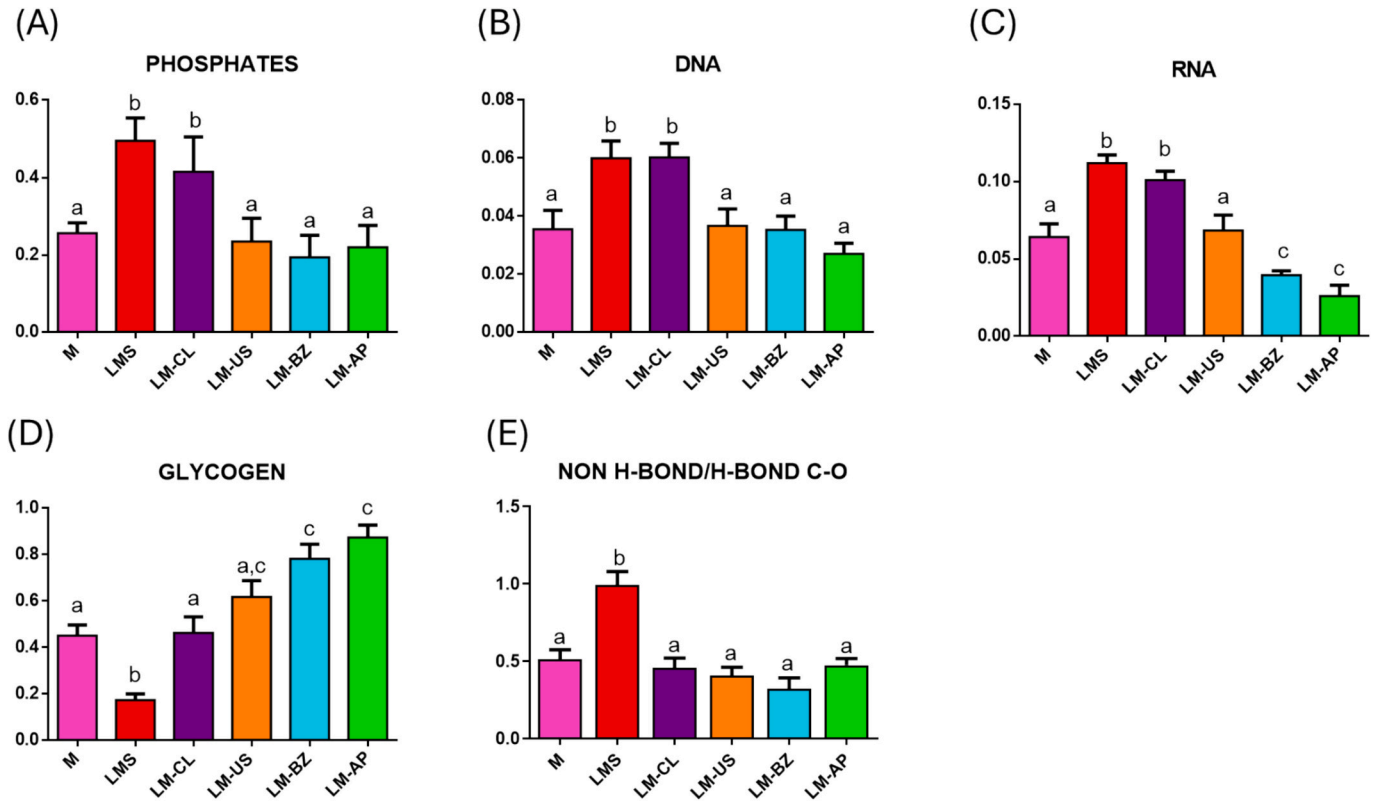


**Fig. 7.** Statistical analysis of the following spectral parameters: (A) PHOSPHATES; (B) DNA; (C) RNA, (D) GLYCOGEN, and (E) NON H-BOND/H-BOND C—O. Data are presented as mean ± SD. Different lowercase letters over histograms indicate statistically significant difference among M, LMS, LM-CL, LM-US, LM-BZ and LM-AP (One-way ANOVA; Tukey's multiple comparisons test; statistical significance was always set at $p < 0.05$; GraphPad software, San Diego, CA).

Histological staining with Masson's Trichrome revealed variable collagen content and distribution among leiomyoma subtypes: LM-US and LM-CL histotypes showed low and patchy collagen deposition, whereas LM-BZ and LM-AP exhibited higher but more irregular collagen distribution. These observations were consistent with IR false color images, which demonstrated elevated collagen and proline content in LM-BZ and LM-AP, compared to LM-US, LM-CL, and LMS. Beyond quantity, the analysis of IR data also revealed differences in collagen organization. The spectral parameters TRIPLE-HELIX, RANDOM, and FOLDED/UNFOLDED, indicative of secondary structure, suggested a more structured matrix in LM-US and LM-CL. Conversely, collagen appeared disorganized in LM-BZ and LM-AP, pointing to altered protein conformation [33].

As for the cellular compartment, LMS displayed the highest levels of nucleic acids (PHOSPHATES, DNA, and RNA parameters), along with reduced glycogen and carbohydrate content (GLYCOGEN parameter). A progressive decrease in nucleic acid signals was observed from LM-CL and LM-US to LM-BZ and LM-AP, evidencing a gradient of proliferative activity. These patterns support the interpretation of LM-US and LM-CL as more cellular subtypes, with LM-US in particular showing

highly proliferative but organized characteristics, while LM-BZ and LM-AP were less cellular but richer in collagen. Interestingly, LMS showed the highest value of the NON H-BOND/H-BOND C—O parameter, while all benign lesions displayed similar and lower values (not statistically significant among them). This finding appears in accordance with what reported in literature [35,36,40,41], regarding the presence of a band at ~1160 $cm^{-1}$ in normal tissues, which shifted to ~1170 $cm^{-1}$ in malignant ones.

FTIR imaging analysis has enabled the differentiation of LMS from LM-BZ. LM-BZ leiomyoma exhibits cells that are morphologically similar to those of LMS and, it is therefore often classified as STUMP in the absence of a definitive diagnosis. Consequently, the ability of FTIR to distinguish between them highlights its potential clinical relevance. Additionally, PCA of the spectral populations of LM-CL and LM-US revealed substantial overlap, along with similar values in several spectral parameters. These findings are consistent with recent literature suggesting that the LM-CL histotype may represent an early developmental stage of LM-US [42,43]. Overall, multivariate analysis (PCA) clearly distinguished LMS from benign leiomyomas, and a set of spectral parameters, collagen content and structure, nucleic acids, and glycosylated compounds, proved effective in highlighting key differences. Notably, while LM-US and LM-CL presented as highly cellular and infiltrative lesions with lower collagen levels, LM-BZ and LM-AP were defined by their dense but disordered extracellular matrix. LMS, by contrast, showed a predominance of cellular components with low collagen, in line with its aggressive behavior. These findings reinforce the hypothesis that both the quantity and organization of collagen, together with cellular metabolic signatures, may be very useful in differentiating uterine smooth muscle tumors. They also support the growing interest in the extracellular matrix's role in tumor development, especially considering recent studies suggesting that an aberrant inflammatory response involving myofibroblasts may drive excessive and disorganized collagen deposition in leiomyomas [44].

## 5. Conclusions

This preliminary study could be considered a proof of concept for the use of the proposed multidisciplinary approach in the differential diagnosis of human uterine muscle lesions. Indeed, the coupling of FTIR Imaging spectroscopy and histology with multivariate and univariate analyses provided complementary information, potentially useful in challenging diagnostic cases. New reliable spectral markers, mainly regarding the relative amount and structure of collagen, nucleic acids, and glycosylated compounds, have been identified, able not only to highlight the malignant nature of the lesion but also to distinguish among the different histological benign variants. We are aware that the variability associated with this kind of samples and the limited number of analyzed specimens could represent some limitation, and, in this regard, further investigations will be carried out to increase the number of cases and to make the proposed spectral markers more robust and generalizable, also including an external validation cohort.

## Declaration of competing interest

The authors declare that they have no known competing financial interests or personal relationships that could have appeared to influence the work reported in this paper.

## Acknowledgments

The Authors thank Dr. Alessia Belloni for her valuable contribution during the acquisition of IR images. C.S. acknowledges the received scholarship (CUP: I32B23001220007), funded under the National Recovery and Resilience Plan (NRRP), Mission 4 “Education and Research”, Component 1 “Enhancement of the offer of educational services: from nurseries to universities”, Investment 4.1 “Extension of the number of research doctorates and innovative doctorates for public administration and cultural heritage” – Ministerial Decree No. 118 of 02/03/2023 adopted by the Italian Ministry of University and Research and funded by the European Union NextGenerationEU.

## Data availability

Data will be made available on request.

## References

[1] N. Wilkinson, T.P. Rollason, Recent advances in the pathology of smooth muscle tumours of the uterus, Histopathology 39 (2001) 331–341, https://doi.org/10.1046/j.1365-2559.2001.01300.x.
[2] D. Day Baird, D.B. Dunson, M.C. Hill, D. Cousins, J.M. Schectman, High cumulative incidence of uterine leiomyoma in black and white women: ultrasound evidence, Am. J. Obstet. Gynecol. 188 (2003) 100–107, https://doi.org/10.1067/mob.2003.99.
[3] P. Ciarmela, G. Delli Carpini, S. Greco, A. Zannotti, N. Montik, L. Giannella, L. Giuliani, C. Grelloni, F. Panfoli, M. Paolucci, G. Pierucci, F. Ragno, P. Pellegrino, F. Petraglia, A. Ciavattini, Uterine fibroid vascularization: From morphological evidence to clinical implications, Reprod. Biomed. Online 44 (2022) 281–294, https://doi.org/10.1016/j.rbmo.2021.09.005.
[4] A.K. Höhn, C.E. Brambs, G.G.R. Hiller, D. May, E. Schmoeckel, L.-C. Horn, WHO classification of female genital tumors, Geburtshilfe Frauenheilkd. 81 (2021) (2020) 1145–1153, https://doi.org/10.1055/a-1545-4279.
[5] P. Ciarmela, S. Islam, P. Lamanna, A. Tranquilli, M. Castellucci, Healthy and pathological changes of myometrium: pregnant myometrium, uterine fibroids and leiomyosarcoma, Rev. Arg. de Anat. Clin. 4 (1) (2012) 7–13, https://doi.org/10.31051/1852.8023.v4.n1.13945.
[6] G. Toledo, E. Oliva, Smooth muscle tumors of the uterus: a practical approach, Arch. Pathol. Lab Med. 132 (2008) 595–605, https://doi.org/10.5858/2008-132-595-SMTOTU.
[7] S. Croce, R.H. Young, E. Oliva, Uterine leiomyomas with bizarre nuclei: a clinicopathologic study of 59 cases, Am. J. Surg. Pathol. 38 (2014) 1330–1339, https://doi.org/10.1097/PAS.0000000000000249.
[8] A. Al-Nafussi, Uterine smooth-muscle tumours: practical approach to diagnosis, Curr. Diagn. Pathol. 10 (2004) 140–156, https://doi.org/10.1016/S0968-6053(03)00072-3.
[9] S.W. Bell, R.L. Kempson, M.R. Hendrickson, Problematic uterine smooth muscle neoplasms: a clinicopathologic study of 213 cases, Am. J. Surg. Pathol. 18 (1994) 535, https://doi.org/10.1097/00000478-199406000-00001.
[10] A. Travaglino, A. Raffone, A. Santoro, D. Raimondo, F.P. Improda, F. Cariati, M. De Marco, P. Casadio, R. Seracchioli, F. Zullo, L. Insabato, G.F. Zannoni, Risk of recurrence in uterine leiomyoma with bizarre nuclei: a systematic review and meta-analysis, Geburtshilfe Frauenheilkd. 81 (2021) 1217–1223, https://doi.org/10.1055/a-1533-1651.
[11] M. Gao, P. Bhosale, C. Devine, S. Palmquist, S. Javadi, US, MRI, CT performance and interpretation of uterine masses, Seminars in Ultrasound, CT and MRI 44 (6) (2023) 541–559, https://doi.org/10.1053/j.sult.2023.10.001.
[12] A. Sahdev, S.A. Sohaib, I. Jacobs, J.H. Shepherd, D.H. Oram, R.H. Reznek, MR Imaging Uterine Sarcomas, Am. J. Roentgenol. 177 (6) (2001) 1307–1311, https://doi.org/10.2214/ajr.177.6.1771307.
[13] I. Thomassin-Naggara, S. Dechoux, C. Bonneau, A. Morel, R. Rouzier, M.-F. Carette, E. Daraï, M. Bazot, How to differentiate benign from malignant myometrial tumours using MR imaging, Eur. Radiol. 23 (8) (2013) 2306–2314, https://doi.org/10.1007/s00330-013-2819-9.
[14] S. Kusunoki, Y. Terao, T. Ujihira, K. Fujino, H. Kaneda, M. Kimura, T. Ota, S. Takeda, Efficacy of PET/CT to exclude leiomyoma in patients with lesions suspicious for uterine sarcoma on MRI, Taiwanese J. Obstetrics and Gynecol. 56 (4) (2017) 508–513, https://doi.org/10.1016/j.tjog.2017.05.003.
[15] E. Oliva, M.L. Carcangiu, S.G. Carinelli, Tumours of the uterine corpus: Mesenchymal tumours: Smooth muscle tumour of uncertain malignant potential, in: R.J. Kurman, M.L. Carcangiu, C.S. Herrington, R.H. Young (Eds.), WHO Classification of Tumors of Female Reproductive Organs, IARC Press, Lyon, 2014, pp. 138–139.
[16] S.R. Guntupalli, P.T. Ramirez, M.L. Anderson, M.R. Milam, D.C. Bodurka, A. Malpica, Uterine smooth muscle tumor of uncertain malignant potential: a retrospective analysis, Gynecol. Oncol. 113 (2009) 324–326, https://doi.org/10.1016/j.ygyno.2009.02.020.
[17] P.P.C. Ip, A.N.Y. Cheung, P.B. Clement, Uterine smooth muscle tumors of uncertain malignant potential (STUMP): a clinicopathologic analysis of 16 cases, Am. J. Surg. Pathol. 33 (2009) 992, https://doi.org/10.1097/PAS.0b013e3181a02d1c.
[18] E. Guo, C. Li, Y. Hu, K. Zhao, Q. Zheng, L. Wang, Leiomyoma with bizarre nuclei: a current update, Int. J. Women's Health 14 (2022) 1641–1656, https://doi.org/10.2147/IJWH.S388278.
[19] S. Croce, F. Chibon, Molecular prognostication of uterine smooth muscle neoplasms: from CGH array to CINSARC signature and beyond, Genes Chromosom. Cancer 60 (2021) 129–137, https://doi.org/10.1002/gcc.22906.
[20] S. Greco, A. Zannotti, P. Pellegrino, F. Giantomassi, G. Delli Carpini, M. D'Agostino, G. Goteri, A. Ciavattini, C. Donati, C. Bernacchioni, F. Petraglia, A. La Teana, P. Ciarmela, High levels of hypusinated eIF5A in leiomyoma and

leiomyosarcoma pathologies: a possible novel therapeutic target, Reprod. Biomed. Online 47 (2023) 15–25, https://doi.org/10.1016/j.rbmo.2023.03.017.
[21] S. Greco, J. Pinheiro, D. Cardoso-Carneiro, F. Giantomassi, P. Pellegrino, G. Scaglione, G. Delli Carpini, A. Ciavattini, G.F. Zannoni, G. Goteri, O. Martinho, P. Ciarmela, Raf kinase inhibitor protein expression in smooth muscle tumours of the uterus: a diagnostic marker for leiomyosarcoma? Reprod. Biomed. Online 48 (2024) 103816 https://doi.org/10.1016/j.rbmo.2024.103816.
[22] L. Togni, M. Furlani, A. Belloni, N. Riberti, A. Giuliani, V. Notarstefano, C. Santoni, E. Giorgini, C. Rubini, A. Santarelli, M. Mascitti, Biomolecular alterations temporally anticipate microarchitectural modifications of collagen in oral tongue squamous cell carcinoma, iScience 27 (2024) 110303, https://doi.org/10.1016/j.isci.2024.110303.
[23] J.D. Pallua, C. Pezzei, B. Zelger, G. Schaefer, L.K. Bittner, V.A. Huck-Pezzei, S. A. Schoenbichler, H. Hahn, A. Kloss-Brandstaetter, F. Kloss, G.K. Bonn, C.W. Huck, Fourier transform infrared imaging analysis in discrimination studies of squamous cell carcinoma, Analyst 137 (17) (2012) 3965, https://doi.org/10.1039/c2an35483g.
[24] M.J. Baker, E. Gazi, M.D. Brown, J.H. Shanks, N.W. Clarke, P. Gardner, Investigating FTIR based histopathology for the diagnosis of prostate cancer, J. Biophotonics 2 (1–2) (2009) 104–113, https://doi.org/10.1002/jbio.200810062.
[25] F. Großerueschkamp, A. Kallenbach-Thieltges, T. Behrens, T. Brüning, M. Altmayer, G. Stamatis, D. Theegarten, K. Gerwert, Marker-free automated histopathological annotation of lung tumour subtypes by FTIR imaging, Analyst 140 (7) (2015) 2114–2120, https://doi.org/10.1039/C4AN01978D.
[26] A. Salman, G. Sebbag, S. Argov, S. Mordechai, R.K. Sahu, Early detection of colorectal cancer relapse by infrared spectroscopy in “normal” anastomosis tissue, J. Biomed. Opt. 20 (7) (2015) 075007, https://doi.org/10.1117/1.JBO.20.7.075007.
[27] S. Farooq, M. Del-Valle, M.O. Dos Santos, S.N. Dos Santos, E.S. Bernardes, D. M. Zezell, Rapid identification of breast cancer subtypes using micro-FTIR and machine learning methods, Appl. Opt. 62 (8) (2023) C80, https://doi.org/10.1364/AO.477409.
[28] S.M. Ali, F. Bonnier, H. Lambkin, K. Flynn, V. McDonagh, C. Healy, T.C. Lee, F. M. Lyng, H.J. Byrne, A comparison of Raman, FTIR and ATR-FTIR micro spectroscopy for imaging human skin tissue sections, Anal. Methods 5 (9) (2013) 2281, https://doi.org/10.1039/c3ay40185e.
[29] H. Fabian, M. Jackson, L. Murphy, P.H. Watson, I. Fichtner, H.H. Mantsch, A comparative infrared spectroscopic study of human breast tumors and breast tumor cell xenografts, Biospectroscopy 1 (1995) 37–45, https://doi.org/10.1002/bspy.350010106.
[30] A. Belloni, M. Furlani, S. Greco, V. Notarstefano, C. Pro, B. Randazzo, P. Pellegrino, A. Zannotti, G. Delli Carpini, A. Ciavattini, F. Di Lillo, E. Giorgini, A. Giuliani, S. Cinti, P. Ciarmela, Uterine leiomyoma as useful model to unveil morphometric and macromolecular collagen state and impairment in fibrotic diseases: an ex-vivo human study, Biochim. Biophys. Acta (BBA) - Mol. Basis Dis. 1868 (2022) 166494, https://doi.org/10.1016/j.bbadis.2022.166494.
[31] E. Barnas, J. Skret-Magierlo, A. Skret, E. Kaznowska, J. Depciuch, K. Szmuc, K. Łach, I. Krawczyk-Marć, J. Cebulski, Simultaneous FTIR and Raman spectroscopy in endometrial atypical hyperplasia and Cancer, Int. J. Mol. Sci. 21 (14) (2020) 4828, https://doi.org/10.3390/ijms21144828.
[32] C. Stani, L. Vaccari, E. Mitri, G. Birarda, FTIR investigation of the secondary structure of type I collagen: new insight into the amide III band, Spectrochim. Acta A Mol. Biomol. Spectrosc. 229 (2020) 118006, https://doi.org/10.1016/j.saa.2019.118006.
[33] C. Licini, V. Notarstefano, S. Marchi, G. Cerqueni, G. Ciapetti, C. Vitale-Brovarone, E. Giorgini, M. Mattioli-Belmonte, Altered type I collagen networking in osteoporotic human femoral head revealed by histomorphometric and Fourier transform infrared imaging correlated analyses, BioFactors 48 (2022) 1089–1110, https://doi.org/10.1002/biof.1870.
[34] S. De Santis, F. Porcelli, G. Sotgiu, A. Crescenzi, A. Ceccucci, M. Verri, M. Caricato, C. Taffon, M. Orsini, Identification of remodeled collagen fibers in tumor stroma by FTIR Micro-spectroscopy: a new approach to recognize the colon carcinoma, Biochim. Biophys. Acta (BBA) - Mol. Basis Dis. 1868 (1) (2022) 166279, https://doi.org/10.1016/j.bbadis.2021.166279.
[35] B. Rigas, S. Morgello, I.S. Goldman, P.T. Wong, Human colorectal cancers display abnormal Fourier-transform infrared spectra, Proc. Natl. Acad. Sci. 87 (20) (1990) 8140–8144, https://doi.org/10.1073/pnas.87.20.8140.
[36] Z. Movasaghi, S. Rehman, Dr.I. Ur Rehman, Fourier transform infrared (FTIR) spectroscopy of biological tissues, Appl. Spectrosc. Rev. 43 (2) (2008) 134–179, https://doi.org/10.1080/05704920701829043.
[37] D. Ami, P. Mereghetti, M. Leri, S. Giorgetti, A. Natalello, S.M. Doglia, M. Stefani, M. Bucciantini, A FTIR microspectroscopy study of the structural and biochemical perturbations induced by natively folded and aggregated transthyretin in HL-1 cardiomyocytes, Sci. Rep. 8 (2018) 12508, https://doi.org/10.1038/s41598-018-30995-5.
[38] V. Notarstefano, S. Sabbatini, C. Conti, M. Pisani, P. Astolfi, C. Pro, C. Rubini, L. Vaccari, E. Giorgini, Investigation of human pancreatic cancer tissues by Fourier transform infrared hyperspectral imaging, J. Biophotonics 13 (4) (2020) e201960071, https://doi.org/10.1002/jbio.201960071.
[39] B.R. Wood, The importance of hydration and DNA conformation in interpreting infrared spectra of cells and tissues, Chem. Soc. Rev. 45 (7) (2016) 1980–1998, https://doi.org/10.1039/C5CS00511F.
[40] R. Campagna, A. Belloni, V. Pozzi, A. Salvucci, V. Notarstefano, L. Togni, M. Mascitti, D. Sartini, E. Giorgini, E. Salvolini, A. Santarelli, L. Lo Muzio, M. Emanuelli, Role played by Paraoxonase-2 enzyme in cell viability, proliferation and sensitivity to chemotherapy of Oral squamous cell carcinoma cell lines, Int. J. Mol. Sci. 24 (1) (2022) 338, https://doi.org/10.3390/ijms24010338.
[41] B.-B. Wu, Y.-P. Gong, X.-H. Wu, Y.-Y. Chen, F.-F. Chen, L.-T. Jin, B.-R. Cheng, F. Hu, B. Xiong, Fourier transform infrared spectroscopy for the distinction of MCF-7 cells treated with different concentrations of 5-fluorouracil, J. Transl. Med. 13 (1) (2015) 108, https://doi.org/10.1186/s12967-015-0468-2.
[42] G.P. Flake, A.B. Moore, D. Sutton, G.E. Kissling, J. Horton, B. Wicker, D. Walmer, S. J. Robboy, D. Dixon, The natural history of uterine leiomyomas: light and electron microscopic studies of fibroid phases, interstitial ischemia, inanosis, and reclamation, Obstet. Gynecol. Int. 2013 (2013) 1–20, https://doi.org/10.1155/2013/528376.
[43] O. Protic, P. Toti, M.S. Islam, R. Occhini, S.R. Giannubilo, W.H. Catherino, S. Cinti, F. Petraglia, A. Ciavattini, M. Castellucci, B. Hinz, P. Ciarmela, Possible involvement of inflammatory/reparative processes in the development of uterine fibroids, Cell Tissue Res. 364 (2016) 415–427, https://doi.org/10.1007/s00441-015-2324-3.
[44] M.S. Islam, A. Ciavattini, F. Petraglia, M. Castellucci, P. Ciarmela, Extracellular matrix in uterine leiomyoma pathogenesis: a potential target for future therapeutics, Hum. Reprod. Update 24 (2018) 59–85, https://doi.org/10.1093/humupd/dmx032.